ACS Catalysis

Research Article

pubs.acs.org/acscatalysis

Effect of Sulfur on Mn/Ti Catalysts Prepared Using Chemical Vapor Condensation (CVC) for Low-Temperature NO Reduction

Eunseuk Park, Minsoo Kim, Hyounduk Jung, Sungmin Chin, and Jongsoo Jurng*

Center for Environment, Health and Welfare Research, Korea Institute of Science and Technology (KIST), 39-1, Hawolgok, Seongbuk, Seoul 136-791, Republic of Korea

ABSTRACT: Mn/Ti catalysts prepared through impregnation of manganese acetate and a manganese nitrate precursor via the chemical vapor condensation (CVC) method were investigated in this study to assess NH_3-selective catalytic reduction (SCR) activity. Manganese (Mn) loaded on a synthesized TiO_2 catalyst showed good low-temperature NO reduction activity and better resistance to sulfur poisoning in presence of SO_2. Mn loaded on synthesized TiO_2 prepared from manganese acetate precursor especially exhibited a high NO conversion of 98.4% at 150 °C. Moreover, it presented high NO conversions within the entire operating temperature window in comparison with other catalysts, which may be attributed to smaller particle size, scattered amorphous Mn over the catalyst surface, higher dispersion, and an abundant Mn_2O_3 phase. X-ray photoelectron spectroscopy (XPS) analysis of the spent catalyst following the SCR reaction in presence of SO_2 verified that the formation of sulfated titanium and manganese sulfate was significantly inhibited, and that the deposition concentration of ammonium sulfate on active sites was low owing to impregnation of Mn acetate onto synthesized TiO_2. FT-IR analysis indicated that the catalyst also contained larger quantities of N−H bonds in NH_3, synchronizing with Lewis acid sites on its surface.

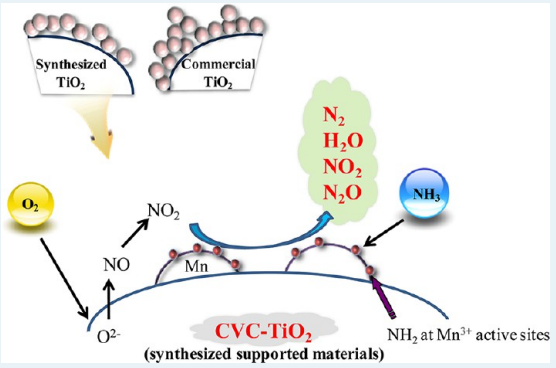

KEYWORDS: *Mn/Ti, chemical vapor condensation, NO reduction, SO_2 poisoning, low-temperature*

1. INTRODUCTION

Selective catalytic reduction (SCR) of nitrogen oxides (NO_x) to N_2 using NH_3 is one of the most effective technologies for the treatment of stack gases from stationary sources such as thermal power plants, waste incinerators, and chemical processes, because of its high removal efficiency and selectivity plus low cost.[1,2] SCR of NO with ammonia generally employs transition metal oxides such as Fe_2O_3, CuO, Cr_2O_3, MnO_2, and their composites with other oxides.[3,4] Although extensively studied, the SCR process still has some disadvantages including low temperature activity and high fuel gas temperature, which may lead to catalyst sintering and deactivation, oxidation of NH_2 to NO, and stack reheating requirements. Moreover, catalyst deactivation is accelerated through exposure to high SO_2 concentrations, and small particulates in coal-fired utility plants.[5] Therefore, it has become essential to develop not only highly active catalysts unaffected by low-temperature SCR but also materials for NO reduction resistant to catalytic deactivation.

Manganese oxide is known for its high activity in SCR of NO at low temperatures.[6−11] Moreover, its amorphous structure implies a large surface area favorable for low temperature SCR. Manganese has many oxidation states, namely, MnO (Mn (II)), Mn_2O_3 (Mn (III)), and MnO_2 (Mn (IV)), and generates a different active site depending on the type of manganese precursors used, leading to variations in its NO reduction performance.[12] A manganese nitrate precursor results primarily in crystal MnO_2, while a manganese acetate precursor results chiefly in a highly dispersed Mn_2O_3 surface. Mn_2O_3 is even better dispersed when prepared at 200 °C, resulting in an improved NO reduction performance as reported by Li et al.[13] However, this catalyst still exhibits low NO conversion properties, is easily deactivated by SO_2, contains H_2O, and requires a broader temperature window.[14,15]

Anatase TiO_2 acts as a stable support in most chemical environments. It is catalytically active because of its high affinity for adsorption of organic pollutants, owing to its higher degree of hydroxylation compared to the rutile phase. In addition, many studies have reported that TiO_2 properties can be enhanced based on its synthesis method.[16,17] Developing nanosized catalysts for NO reduction and MnO_x/TiO_2 nanocomposites prepared by the solution impregnation method are the focus of many low-temperature NO reduction studies. However, conventional impregnation of Mn/TiO_2 generally results in poorly dispersed manganese oxide and causes amorphous manganese oxide to transform into its crystalline form. Additionally, pore sizes and surface areas of the resulting mesoporous material, distributed mainly on the inner

Received: December 4, 2012
Revised: May 22, 2013
Published: May 30, 2013

surfaces often decrease because of blockage, following reagent loading.[18] Recent studies[19,20] have focused on Mn loaded on TiO_2 prepared by the impregnation method using chemical vapor condensation (CVC). The resulting Mn/TiO_2 in these studies was found to show good catalytic activity for toluene, owing to its good surface dispersion, large surface area, and the presence of nanoscale oxides in its structure.

In this study, anatase TiO_2 particles were synthesized using CVC, and subsequently loaded with manganese via impregnation of manganese acetate and manganese nitrate precursors. The effect of using different Mn precursors on the Mn/TiO_2, and the effect of deactivating agent such as SO_2 and H_2O, on low-temperature NO reduction activity were studied. The NO reduction activity of this catalyst was also compared with that of catalysts prepared using Mn impregnation on commercial TiO_2 (P25) without employing CVC.

2. EXPERIMENTAL SECTION

2.1. Samples and Their Characterization. In this study, TiO_2 particles synthesized using the CVC process at a temperature of 900 °C were used as the support (the schematic of which is provided in our previous study).[21] Mn/TiO_2 catalysts were prepared via the impregnation method using aqueous solutions of manganese nitrate ($Mn(NO_3)_2$, 99.99%, Aldrich) and manganese acetate tetrahydrate ($Mn(CH_3COO)_2$ $4H_2O$, Aldrich, 99.99%) as the metal precursors. The concentration of manganese precursors was fixed at 10 wt % on the TiO_2-support. The catalyst samples were dried overnight at 110 °C, and calcined at 500 °C for 2 h in static air. The obtained catalyst samples were labeled as "Mn(manganese precursor)/(prepared type)Ti(after reaction)." For example, a sample produced via CVC, using the manganese acetate precursor was labeled Mn(A)/CVCTi, while a sample post-reaction in the presence of 200 ppm SO_2 for 15 h was denoted as Mn(A)/CVCTi(S). Degussa P25, unloaded titania, and manganese oxide-loaded on P25 were used as reference catalysts for comparison.

X-ray diffraction (XRD) was performed using a high-resolution X-ray diffractometer (focal spot size: 5 mm^2, Cu rotating anode). High-resolution transmission electron microscopy (HR-TEM) was conducted using an F-20 microscope (Philips; operated at 200 kV, image resolution <0.25 nm). The specific surface areas (SSA, $m^2\ g^{-1}$) of powdered samples were determined through nitrogen adsorption (>99.999%) at 77 K (Micromeritics Tristar 3000 apparatus) using the Brunauer–Emmett–Teller (BET) method. Pore volume distributions were determined from desorption isotherms (Micromeritics ASAP 2010 Multigas system) using the Barrett–Joyner–Halenda (BJH) method. Particle sizes (d_{XRD}) were estimated using the Scherrer equation, assuming monodispersed spherical primary particles. X-ray photoelectron spectroscopy (XPS) (VG scientific ESCA Lab II Spectrometer (resolution 0.1 eV)) was conducted using Mg Kα (1253.6 eV) radiation as the excitation source. FT-IR (Thermo Mattson Infinity Gold FT-IR series equipment) was used to obtain spectra of powdered samples.

2.2. Activity Measurements. NO reduction activity tests were carried out in a fixed-bed flow reactor with an inner diameter of 6.5 mm and a height of 400 mm. The space above and below the catalyst layer was filled with quartz wool to secure it and to minimize channeling. Gas flow was controlled using mass-flow meters. The simulated flow rate of the flue gas was set at 400 mL min^{-1} and one atmospheric pressure, corresponding to a gas hour space velocity (GHSV) of 30,000 h^{-1}. The reaction temperature of the catalytic bed was varied from 50 to 400 °C at 50 °C intervals. A reaction mixture contained 5% O_2, with 500 ppm NO and N_2 comprising the rest of the mixture, and 0.1 g of sample was employed in each run. The $[NH_3]/[NO]$ ratio was increased from 0.5 to 1.5 stoichiometrically. A 10 vol % H_2O vapor and 200 ppm SO_2 were added to the reaction stream to test catalyst resistance. NO_x and SO_2 concentrations were measured using a NO/NO_x analyzer (GreenLine MK9000, Eurotron Corp). The concentrations of gaseous N_2O and N_2 were analyzed using a gas chromatograph equipped with a HP-PLOT 5A and a TCD detector. The conversion of NO was calculated as $([NO]_{in} - [NO]_{out})/[NO]_{in}$, and N_2 selectivity was calculated as $[N_2]/[N_2] + [N_2O] + [NO_2])$.

3. RESULTS AND DISCUSSION

3.1. Catalytic Performance in Low-Temperature SCR. Figure 1 shows NO reduction efficiency obtained using

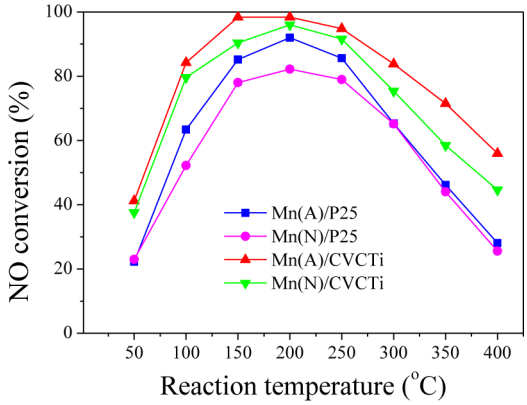

Figure 1. NO conversion by SCR over TiO_2 and Mn/Ti catalysts (GHSV = 30,000h^{-1}, $[O_2]$ = 5%, $[NH_3]/[NO]$ = 1.2, and balance N_2).

catalysts produced through the two kinds of Mn precursors with reaction temperatures varying from 50 to 400 °C. The results indicate that temperature has a significant effect on NO reduction activity. A negligible NO conversion was observed over naked CVCTi and P25 supports at all temperatures, whereas dispersing Mn onto TiO_2 resulted in an improved activity in SCR of NO. The NO reduction efficiency in all catalysts initially increased, stabilized intermediately, but subsequently decreased with an increase in temperature. The N_2 selectivity of all samples was found to be equal at 100%, irrespective of catalytic activity. Within the reaction temperature range and even at lower temperatures, Mn/CVCTi showed a higher efficiency than Mn/P25, regardless of the Mn precursor used. These results indicate that the addition of Mn improved low-temperature activity, and that the CVCTi support material caused an enhanced NO reduction activity in the catalyst. Mn(A)/CVCTi showed the highest NO reduction activity of 98.4% at 150 °C. NO conversion in Mn(A)/P25, on the other hand, was found to increase slowly with rising temperature, and reached a maximum of 92% at 200 °C. The higher catalytic activity of Mn(A)/CVCTi may be attributed to the presence of abundant Mn_2O_3, which increases its reduction ability and improves NO conversion activity at low temperatures.[12,19]

dx.doi.org/10.1021/cs3007846 | ACS Catal. 2013, 3, 1518–1525

Figure 1 also shows that Mn(A)/CVCTi has the largest temperature window of approximately 100−400 °C, while Mn(A)/P25 shows an NO reduction activity of over 80% only in the temperature window of 150−250 °C. Yu et al.[22] reported that Mn-based catalysts prepared via the impregnation method exhibited higher activities at temperatures below 200 °C, but deactivated at high temperatures, owing to low dispersion of active components and formation of crystal grains on the catalyst surface, which they determined using XRD and XPS analyses. Impregnated manganese acetate precursor on CVCTi delivered the best NO reduction catalyst performance in the reaction temperature window. Low reduction temperatures observed in this case indicates the presence of a Mn_2O_3 phase at this reaction temperature. Moreover, the good dispersion behavior of amorphous Mn on the catalyst surface reduces catalytic deactivation at high temperatures.

In general, N_2O is formed via NH_3 oxidation in SCR of NO. Figure 2 shows N_2O concentrations and NH_3 conversions at

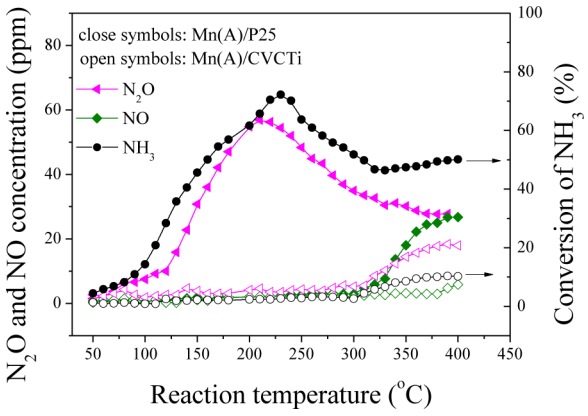

Figure 2. Trend of forming N_2O and NO in oxidizing NH_3 on Mn(A)/CVCTi and Mn(A)/P25 catalysts (NH_3: 150 ppm, GHSV = 30,000 h^{-1}, $[O_2]$ = 5%).

various reaction temperatures in the range of 50 to 400 °C, with the catalysts Mn(A)/CVCTi and Mn(A)/P25. There was an obvious formation of N_2O over Mn-loaded P25, but the N_2O concentration was very low until 250 °C over Mn-loaded CVCTi. Further, N_2O concentration on Mn(A)/CVCTi was not detected until 350 °C. Figure 2 also shows that the initial NO concentration peak over Mn/P25 was observed at 300 °C, and its height increased with increasing reaction temperature. However, in the case of Mn/CVCTi, NO formation was very limited at all temperatures, and N_2O was detectable only at temperatures over 300 °C. These results indicate that the oxidation of NH_3 into N_2O and NO was almost negligible and that the catalyst structure (Mn loaded on different TiO_2 support materials) determines the NH_3 oxidation activity. Moreover, clearly, the highly dispersed M_2O_3 on CVCTi greatly suppressed the NH_3 oxidation activity.

The difference in the behavior between the Mn/CVCTi and the Mn/P25 samples in the dispersion of active components and the interaction of manganese oxides on the catalyst surface are presented in subsequent sections.[22]

NH_3 concentration also plays an important role in the catalytic activity of NO with NH_3.[23] Therefore, the effect of $[NH_3]/[NO]$ ratio in the range of 0.5−1.5 on the NO reduction catalytic efficiency in Mn/Ti catalysts was investigated in this study. Ammonia is initially adsorbed and transformed to amine species on the catalyst surface, and subsequently reacts with NO. Excessive NH_3, however, not only reacts with nitric and sulfuric acids to form ammonium sulfate and ammonium nitrate salts, but also gets adsorbed on the catalyst surface and is released at high temperatures, leading to the presence of undesirable particulate matter and odor.[24] An $[NH_3]/[NO]$ ratio of 1 is generally considered optimal according to the stoichiometric reaction between NO and NH_3 to N_2. Figure 3 shows that NO conversion increases with the

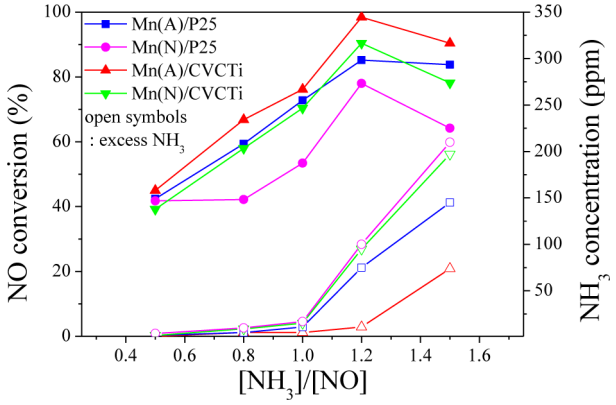

Figure 3. Effect of $[NH_3]/[NO]$ on NO conversion over Mn(A)/Ti and Mn(N)Ti catalysts (temperature =150 °C, GHSV = 30,000 h^{-1}, $[O_2]$ = 5%, [NO] = 500 ppm).

$[NH_3]/[NO]$ ratio. NO conversion of Mn(A)/CVCTi was found to be practically absent when $[NH_3]/[NO]$ is 1.2, which is also the point of maximum efficiency at 98%. With $[NH_3]/[NO]$ ratios greater than 1.2, NO conversion was found to drop because of an increase in NH_3 concentration. At low $[NH_3]/[NO]$ ratios, NH_3 could be adsorbed onto the catalyst and react with NO; excess NH_3 concentration, however, limits the adsorbed sites.[23] Figure 3 shows excess NH_3 in all samples with an initial $[NH_3]/[NO]$ ratio greater than 0.8 that increases rapidly with NH_3 concentration and attains a maximum at 210 ppm. In contrast, Mn/CVCTi catalyst showed too low excess NH_3 concentration, even when the $[NH_3]/[NO]$ ratio is 1.2. Excess NH_3 concentration was found to be lowest in Mn(A)/CVCTi compared to other catalysts in the entire range indicating that the CVCTi support particles improve NO reduction activity of the material probably owing to abundant surface sites and higher surface area, leading to a higher NH_3 absorption ability.[25]

3.2. Catalyst Characterization. Figure 4 shows the X-ray diffraction patterns of the Mn/Ti powdered catalyst formed from the different Mn precursors. The diffractogram patterns of pure TiO_2 are also presented for comparison. Figure 5 shows that in commercial P25 and Mn/P25, anatase and rutile phases were detected. Following manganese nitrate and manganese acetate impregnation, several new diffraction peaks were found to appear in the oxides MnO_x in Mn/P25. On the other hand, in CVCTi and Mn loaded on CVCTi, only anatase phase (JCPDS #71-1169) peaks were detected (2θ = 25.3°, 38.1°, and 48.2°), and MnO_x phase peaks were absent, which may be because of the introduction of Mn into the catalyst causes the active phase to be well dispersed over CVCTi regardless of the Mn precursor. A previous study[18] reported that crystalline phases of manganese oxides form in manganese loadings greater than 10%. Accordingly, in the case of Mn loaded on the CVCTi surface there may have been a greater contact between

dx.doi.org/10.1021/cs3007846 | ACS Catal. 2013, 3, 1518−1525

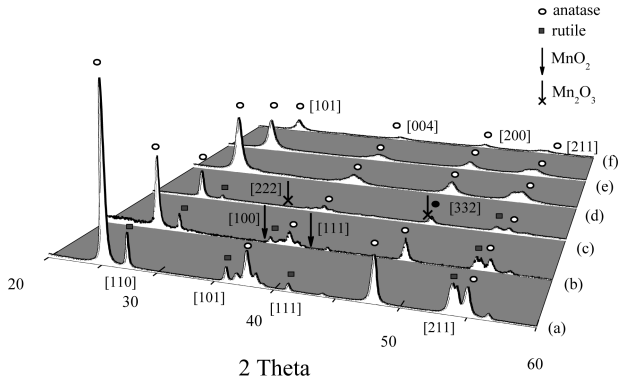

Figure 4. XRD patterns of TiO_2 and Mn/Ti catalysts (a) P25; (b) Mn(N)/P25; (c) Mn(A)/P25; (d) CVCTi; (e) Mn(N)/CVCTi; (f) Mn(A)/CVCTi.

TiO_2 and manganese oxides, since these oxides are well dispersed on the support material. Moreover, the amorphous phase of Mn and TiO_2 anatase is more conducive to SCR activity.[5,26,27] It has been reported that the presence of amorphous (Mn) is related to active component dispersion, and low crystallinity, leading to low sintering and high activity.[23] From these results pertaining to Mn/CVCTi, it is possible that more MnO_x is dispersed in the amorphous phase in the catalyst, thus leading to higher activity.

The physicochemical properties of Mn/Ti produced using the two different kinds of Mn precursor are summarized in Table 1. Previous studies[13,28] have reported that surface area and pore volume decrease in supports impregnated with manganese oxide precursors. However, as seen in Table 1, impregnation of CVCTi with manganese acetate and manganese nitrate precursors increase surface area and pore volume, regardless of Mn precursor. Mn(A)/CVCTi was found to possess the highest surface area and pore volume of 226.8 m^2 g^{-1} and 0.407 cm^3 g^{-1}, respectively. In comparison, the impregnation of Mn acetate precursor on commercial P25 was found to possess a surface area and pore volume of 48.9 m^2 g^{-1} and 0.246 cm^3 g^{-1}, respectively. This difference may occur owing to differences in pore formation between the catalysts. Furthermore, Mn loading also has an effect on the pore size of Mn/P25, whereas Mn/CVCTi does not change pore size. This may indicate that loading manganese oxide on the pores of Mn/P25 surface leads to filling and blockage, causing a decrease in surface area of Mn/P25 compared to commercial P25. This result was also reported by Park et al.[25]

Table 1. Properties of TiO_2 and Mn/Ti Catalysts

sample	BET surface area (m^2 g^{-1})	average pore size (nm)	pore volume (cm^3g^{-1})	average particle size (nm)[a]
P25	51.6	20.01	0.304	29.5
Mn(A)/P25	48.9	41.21	0.246	30.9
Mn(N)/P25	43.6	39.52	0.186	33.2
CVCTi	110.3	3.13	0.140	12.1
Mn(A)/CVCTi	226.8	3.49	0.407	6.0
Mn(N)/CVCTi	198.6	4.13	0.282	7.7

[a]Calculated by the Scherrer formula.

Figure 5 shows TEM images of microstructures of Mn loaded on TiO_2. The morphology and size of both P25 and Mn/P25 was found to increase marginally both prior to and following Mn precursor impregnation, indicating that the Mn is poorly dispersed and causes sintering. Particle sizes of these samples ranged from 25 to 35 nm, and were found to agree with crystallite sizes determined by XRD spectra. On the other hand, with manganese oxide impregnation, Mn/CVCTi sizes were found to decrease from 12.1 to 6.0 nm, regardless of Mn precursor, indicating improved surface area and strong interactions between Mn and Ti.[29] Hence, the Mn(A)/CVCTi fine particle catalyst may possess large surface areas and better dispersion of the active component. This corresponds to the results from BET measurements. The higher NO reduction efficiency of Mn(A)/CVCTi compared to

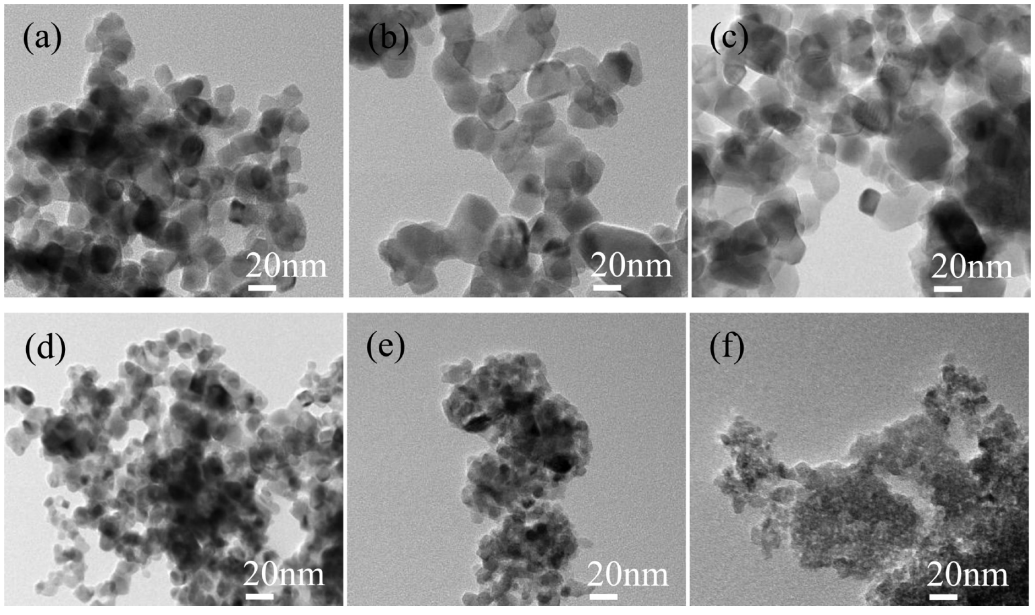

Figure 5. TEM image of TiO_2 and Mn/Ti catalysts (a) P25; (b) Mn(N)/P25; (c) Mn(A)/P25; (d) CVCTi; (e) Mn(N)/CVCTi; (f) Mn(A)/CVCTi.

dx.doi.org/10.1021/cs3007846 | ACS Catal. 2013, 3, 1518−1525

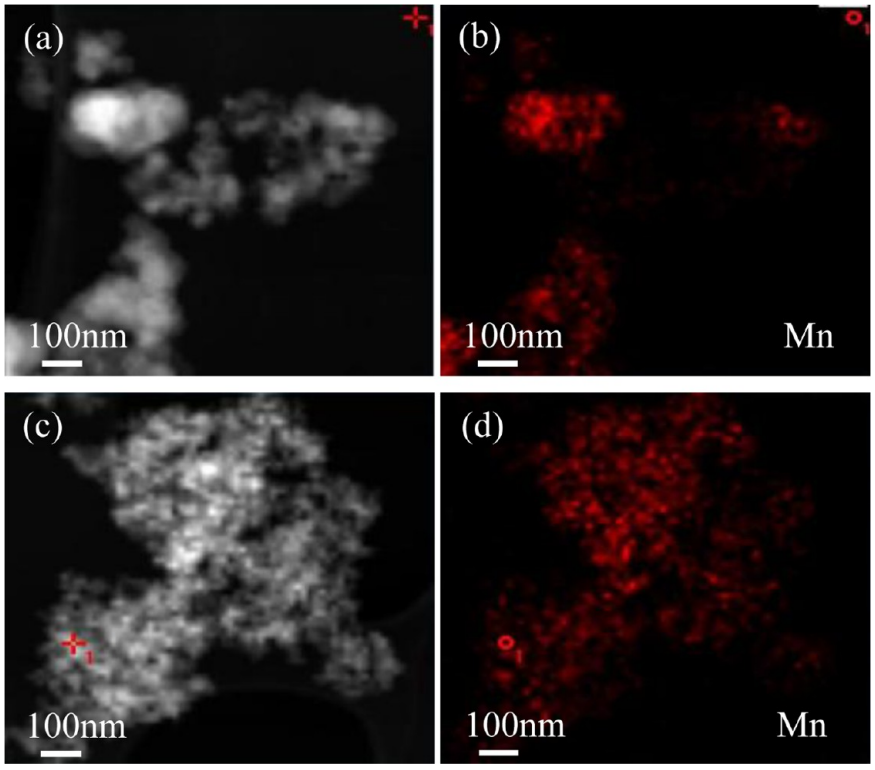

Figure 6. EDX images of Mn/Ti catalysts. (a,c) High-angle annular dark field image of Mn(A)/P25 and Mn(A)/CVCTi; (b,d) Mn elemental spots of Mn(A)/P25 and Mn(A)/CVCTi.

Mn(A)/P25 may be due to the higher dispersion of Mn on the surface of the catalyst.[18]

Figure 6 shows EDX mapping images of Mn(A)/CVCTi and Mn(A)/P25 used to investigate ion dispersion of the metal loaded TiO_2 catalysts. Moreover, the amorphous form of Mn may be more scattered over the CVCTi support compared to Mn-MA/Ti−P25 as seen in Figure 6 (b, d). This is also consistent with the XRD patterns shown in Figure 4. Amorphous structure is also considered to be favorable to low temperature SCR.[30] Based on these results, Mn(A)/CVCTi and Mn(A)/P25 were selected for further characterization in investigating the effect of the H_2O and SO_2 on SCR activity.

3.3. Effect of H_2O and SO_2 on SCR. Catalyst deactivation by residual SO_2 occurs because of its presence in the flue gas in low concentrations even after desulfurization. Figure 7 shows the combined impact of SO_2 and H_2O on NO reduction efficiency in Mn/Ti. The NO conversion of Mn(A)/CVCTi and Mn(A)/P25 is 53% and 83%, respectively, in the absence of SO_2 and H_2O. NO conversion was found to decrease following the addition of steam to the stream, indicating that steam and NH_3 compete for active sites, consequently leading to a decrease in NO conversion.[31] Introducing 200 ppm of SO_2 into the flue gas was found to cause a decrease in NO conversions from 70% to approximately 58% in 250 min at 100 °C in Mn(A)/CVCTi. In Mn(A)/P25 a sharp decline in NO conversion from 38% to approximately 10% in 30 min was observed under similar conditions. The introduction of SO_2 only marginally decreases NO conversion in Mn(A)/CVCTi, implying that this catalyst has a greater reduction in activity compared to Mn(A)/P25.

Figure 7 also shows outlet concentrations of SO_2. SO_2 concentration was found to increase with reaction time before

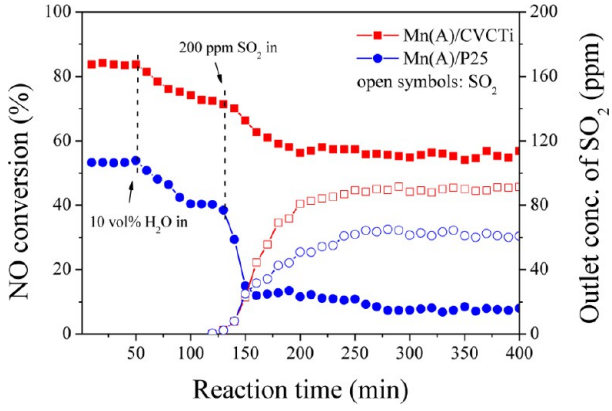

Figure 7. Effect of steam and SO_2 on NO conversion of Mn/Ti catalysts (H_2O = 10 vol %, SO_2 = 200 ppm, NO = 500 ppm, $[NH_3]/[NO]$ = 1.2, O_2 = 5%, temperature =100 °C, GHSV = 30,000 h^{-1} and balance N_2).

approaching a steady value. This indicates formation of ammonium sulfate in the reaction between SO_2 and NH_3 in the Mn catalyst. In Mn(A)/CVCTi, outlet SO_2 concentration was found to be marginally higher than that of Mn-MA/P25, indicating that the sulfate adsorbed on active sites decreases, and consequently inhibits the effect of SO_2 on reduction activity. Huang et al.[32] reported that the adsorption of SO_2 is stronger than NO and forms a sulfite ion on the catalyst surface. The adsorbed sulfite ion and adsorbed oxygen result in sulfate formation, leading to block active component contact with reactive substances and causing a decline in activity. Therefore, the impact of SO_2 on catalyst performance is more significant than that of H_2O. Moreover, Mn(A)/CVCTi was found to exhibit better SO_2 and H_2O poisoning resistance,

dx.doi.org/10.1021/cs3007846 | ACS Catal. 2013, 3, 1518−1525

possess more active sites, and better reduction activity compared to other samples. More study results are presented in subsequent sections.

3.4. XPS and FT-IR Analyses. To identify the state of surface and SO_2 poison-inducing species following SCR, Mn 2p, Ti 2p, O 1s, and S 2p photoelectron peaks of the samples were measured using XPS, and their surface atomic content is presented in Table 2.

Table 2. XPS Results of Catalysts

	surface atomic content (atom %)				
samples	Mn	Ti	O	S	Mn/Ti
P25		28.96	71.04		
Mn(A)/P25	10.28	25.03	64.70		0.15
Mn(A)/P25(S)	6.07	23.11	68.31	2.49	0.26
CVCTi		27.59	72.41		
Mn(A)/CVCTi	11.90	24.54	63.55		0.18
Mn(A)/CVCTi(S)	9.19	23.3	66.51	1.00	0.36

Figure 8 shows the Mn, Ti, O, and S photoelectron peaks of the impregnated Mn acetate precursor on TiO_2. Mn(A)/P25 has a higher surface atomic ratio of Mn compared to Mn(A)/CVCTi, despite their equal 10 wt % Mn loadings. This may imply that the introduction of Mn is highly dispersed on the surface of the CVCTi catalysts whereas sintered over P25.[13] The amount of impregnated Mn on support materials is related to the dispersion of Mn. Figure 8(a) shows the XPS spectra of Mn 2p in fresh and spent catalysts. The binding energies of Mn 2p were found to be similar in Mn(A)/Ti and Mn(A)/Ti(S), with Mn $2p_{3/2}$ and Mn $2p_{1/2}$ as 641.5 and 653 eV, respectively. The Mn $2p_{3/2}$ peak in Mn(A)/P25 was found to be broad, a characteristic of a mixed-valence Mn^{3+} (641.2 ± 0.2 eV) and Mn^{4+} (642.7 ± 0.2 eV) state. Delimaris et al.[33] reported that manganese oxide undergoes oxidation−reduction cycles (redox) in these reactions; therefore, Mn^{3+} and its redox process may be the reason for high activity in the SCR reaction of NO with NH_3 at low temperatures. These results also corroborate the aforementioned XRD and Mn $2p_{3/2}$ Gaussian−Lorentzian curve fitting results. Moreover, the primary peak of Mn $2p_{3/2}$ in Mn(A)/P25 was found to show a binding energy shift by 0.6 eV after reactions in SO_2 containing gas, indicating

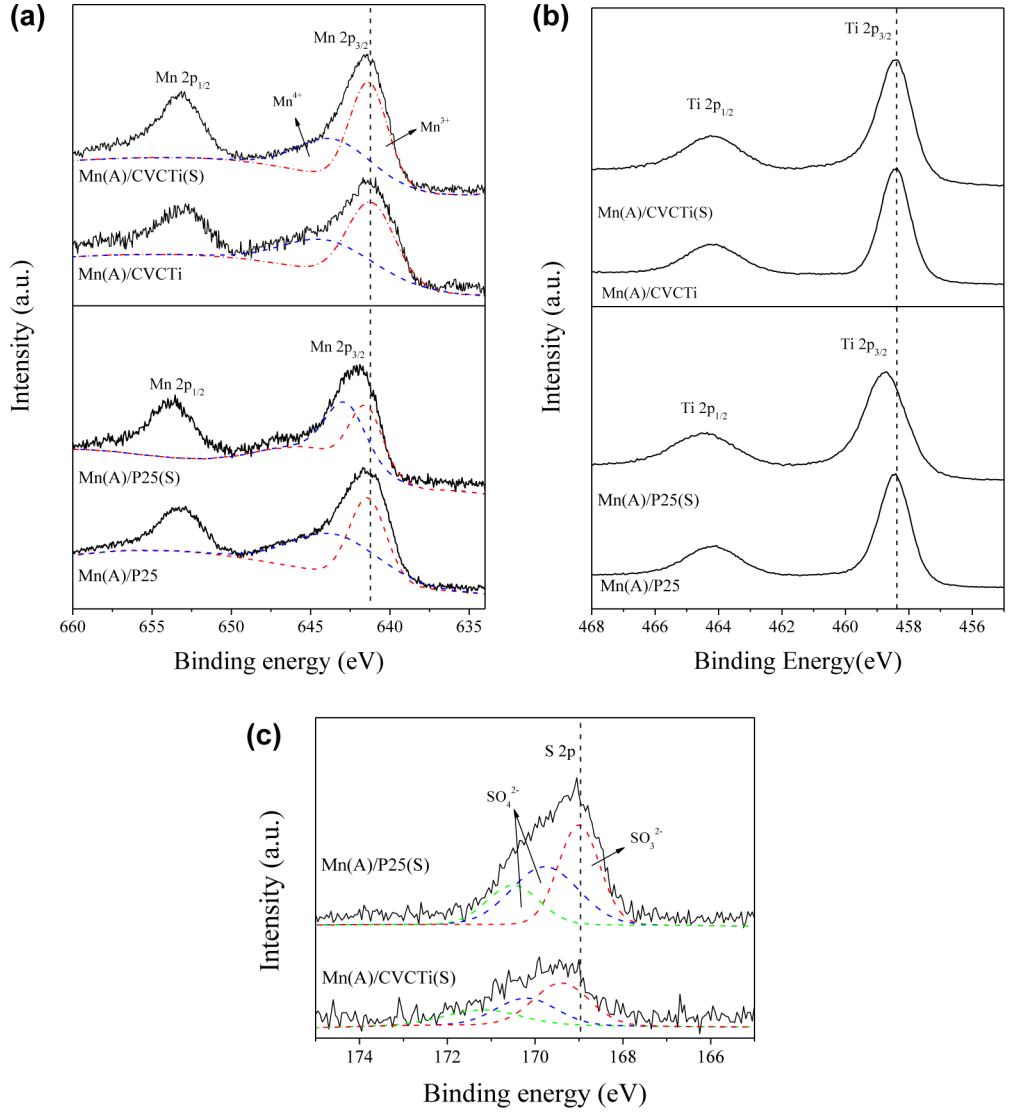

Figure 8. XPS spectra of Mn/Ti catalysts (a) Mn 2p; (b) Ti 2p; (c) S 2p.

dx.doi.org/10.1021/cs3007846 | ACS Catal. 2013, 3, 1518−1525

that a surface species other than MnO_x formed in Mn(A)/P25(S); similar results were reported by Wu et al.[34] On the other hand, in Mn(A)/CVCTi, no binding energy shift was detected. In Mn(A)/P25, the content of Mn was found to decrease sharply from 10.28% to 6.07%. In contrast, the content of Mn and Ti in Mn(A)/CVCTi only decreased marginally following SCR in the presence of SO_2 (Table 2). This indicates that dispersion or surface atomic content of Mn on the CVCTi catalyst support surface is higher than that of commercial P25, and that Mn_2O_3 but not $MnSO_4$ exists stably on its surface. The impregnation of Mn on CVCTi catalyst may therefore occur chiefly because of the deposition of ammonium sulfate on active sites rather than because of the formation of $MnSO_4$, and this leads to minor catalytic deactivation.[25] Figure 8(b) indicates that the binding energies of Ti $2p_{3/2}$ and Ti $2p_{1/2}$ on the surfaces of fresh and spent catalysts emit signals at 458.5 and 464.3 eV, respectively. They consist of only of Ti^{4+} (TiO_2) with a peak separation of 5.8 eV, corresponding with the values reported in our previous study.[35] The binding energy of Ti 2p was found to be unaltered following SCR in Mn(A)/CVCTi(S). Mn(A)/P25(S), however, showed a minor binding energy shift by 0.2 eV, indicating the formation of sulfated titanium, causing faster catalytic deactivation; although, the Mn loaded on CVCTi may prevent TiO_2 from being sulfated. Figure 8(c) shows that there is a negligible difference between XPS spectra of S 2p at a binding energy of 169.1 eV in fresh and spent catalysts. The S 2p peaks was found to overlapped in three regions; the first peak (ca. 168.5 eV) in the S 2p region corresponds to surface SO_3^{2-} formation, the second and third (ca. 169.2 and 169.7 eV) correspond to surface SO_4^{2-} formation.[36] Compared to Mn(A)/CVCTi(S) spectra, however, the spectrum intensity of S 2p became lower after reactions in SO_2 containing gas, indicating a decrease in S surface atomic content (Table 2). Thus, Mn(A)/CVCTi was found to show lower surface concentrations of sulfite and sulfate species, indicating that impregnation of Mn acetate onto CVCTi results in better catalytic deactivation in the presence of SO_2 in the reactant gas.

FT-IR spectroscopy was used to understand the surface poisoning effect in the reaction by examining SO_2 adsorption and deactivation. Figure 9 shows FT-IR spectra of fresh and spent Mn(A)/Ti. The used catalyst was obtained from flue gas SO_2 tests. All spectra were normalized and recorded under identical operating conditions. The spectra of all catalysts exhibit vibration absorption, a strong peak at approximately 500 cm^{-1}, and a weak peak at 3421 cm^{-1}, as a result of stretching vibrations of Ti−O and O−H.[37] The FT-IR spectrum of Mn(A)/P25(S) catalyst was found to show two strong absorption peaks at 510 cm^{-1} and 640 cm^{-1}, owing to TiO_2-rutile phase. Mn(A)/CVCTi(S) was found to show an absorption peak at 600 cm^{-1} (between 450 cm^{-1} and 750 cm^{-1}) corresponding to TiO_2-anatase phase.[38] A new IR band of Mn(A)/Ti spent catalyst was seen at 1414 cm^{-1}, caused by $(NH_4)_2SO_4$, chemisorbed on Brønsted acid sites.[22] Absorption was also seen at 1140 cm^{-1} in the used catalyst, corresponding to SO_4.[2,39] At 1414 $cm^{-1}$and 1140 cm^{-1}, the IR absorption peaks of Mn(A)/CVCTi(S) were found to show lower intensity and were broader compared to Mn(A)/P25(S), which may be due to the overlap of the narrow band of SO_4^{2-}, indicating that Mn(A)/CVCTi(S) was not deactivated considerably. In Mn-MA/P25, ammonium sulfate barely decomposes owing to the slow diffusion of NO in the catalyst making deposition faster than decomposition, and consequently causes the catalyst to deactivate unceasingly.[22]

The absorption peak at 1165 cm^{-1} in Mn(A)/CVCTi(S) was clearly broader, and the peak at 3123 cm^{-1} was found to be stronger compared to that in Mn(A)/P25(S), owing to symmetric bending vibrations of N−H in NH_3 corresponding to Lewis acid sites. Moreover, a small shoulder was found at approximately 1550 cm^{-1}, caused by an amide (NH_2).[40] NH_3 is preferentially adsorbed at Mn^{3+} sites which subsequently forms NH_2 by H-abstraction, followed by a reaction between NH_2 and NO to produce N_2 and H_2O.[13,41] It can be concluded from these results that the Mn(A)/CVCTi catalyst shows better resistance to sulfur, and that an abundance of Lewis acidity on the Mn(A)/CVCTi surface, which has a significant effect on the reaction, may improve low-temperature NH_3−SCR activity of NO.

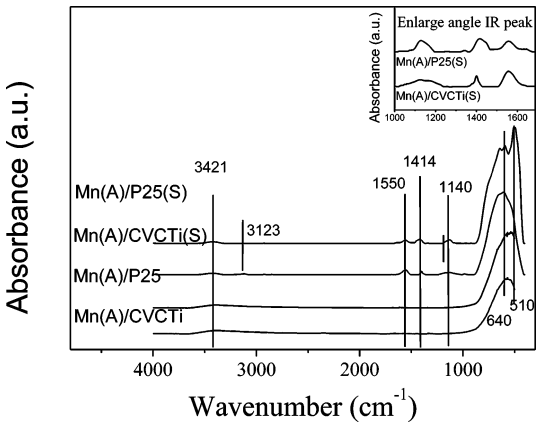

Figure 9. FT-IR spectrum of a few typical fresh and spent catalysts.

4. CONCLUSIONS

Mn/TiO_2 catalysts were prepared through the impregnation of two different precursors, manganese acetate and manganese nitrate, on TiO_2 fabricated by CVC. The catalytic activity of Mn/TiO_2 in NO SCR, and deactivation by residual SO_2 were significantly different in the low-temperature region. Mn(A)/CVCTi possessed abundant amorphous Mn_2O_3 quantities, had no pore blocking, low crystallinity, and good dispersion of the active component, and showed the highest NO reduction activity at low-temperatures compared to other catalysts. This catalyst also showed a wide temperature window, and exhibited high NO conversions. When induced with SO_2, Mn(A)/CVCTi was found to have better resistance to the gas. This could inhibit catalyst poisoning by sulfate species, such as $Ti(SO_4)_2$ and $Mn(SO_4)_x$, and inhibit the formation of ammonium sulfate on the catalyst surface. Moreover, FT-IR showed many Lewis acid sites and minimal decomposition of ammonium sulfate in the Mn(A)/CVCTi catalyst compared to Mn(A)/P25; these properties cause the former catalyst to possess a good NO reduction activity at low temperatures as well as lower catalytic deactivation in presence of SO_2.

AUTHOR INFORMATION

Corresponding Author

*E-mail: jongsoo@kist.re.kr.

Notes

The authors declare no competing financial interest.

■ ACKNOWLEDGMENTS

This work has been supported by the Ministry of Environment (192-091-001), the Ministry of Education, Science and Technology (2011K000750), and the Korea Institute of Science and Technology (KIST) Institutional Program (2E23952).

■ REFERENCES

(1) Nova, I.; Acqua, L. D.; Lietti, L.; Giamello, E.; Forzatti, P. *Appl. Catal., B* **2001**, *35*, 31−42.
(2) Casagrande, L.; Lietti, L.; Nova, I.; Forzatti, P.; Baiker, A. *Appl. Catal., B* **1999**, *22*, 63−77.
(3) Busca, G.; Lietti, L.; Ramis, G.; Berti, F. *Appl. Catal., B* **1998**, *18*, 1−36.
(4) Wu, Z.; Jin, R.; Liu, Y.; Wang, H. *Catal. Commun.* **2008**, *9*, 2217−2220.
(5) Ettireddy, P. R.; Ettireddy, N.; Mamedov, S.; Boolchand, P.; Smirniotis, P. G. *Appl. Catal., B* **2007**, *76*, 123−134.
(6) Thirupathi, B.; Smirniotis, P. G. *Appl. Catal., B* **2011**, *110*, 195−206.
(7) Billik, P.; Plesch, G. *Mater. Lett.* **2007**, *61*, 1183−1186.
(8) Shen, B.; Ma, H.; Yao, Y. *J. Environ. Sci.* **2012**, *24*, 499−506.
(9) Sultana, A.; Sasaki, M.; Hamada, H. *Catal. Today* **2012**, *185*, 284−289.
(10) Baláž, P.; Boldižárová, E.; Godočíková, E.; Briančin. *J. Mater. Lett.* **2003**, *57*, 1585−1589.
(11) Thirupathi, B.; Smirniotis, P. G. *J. Catal.* **2012**, *288*, 74−83.
(12) Ko, J. H.; Park, S. H.; Jeon, J. K.; Kim, S. S.; Kim, S. C.; Kim, J. M.; Chang, D.; Park, Y. K. *Catal. Today* **2012**, *185*, 290−295.
(13) Li, J.; Chen, J.; Ke, R.; Luo, C.; Hao. *J. Catal.Commun.* **2007**, *8*, 1896−1900.
(14) Bhatia, D.; McCabe, R. W.; Harold, M. P.; Balakotaiah, V. *J. Catal.* **2009**, *266*, 106−119.
(15) Li, L. D.; Shen, Q.; Cheng, J.; Hao, Z. P. *Appl. Catal., B* **2010**, *93*, 259−266.
(16) Tian, G.; Fu, H.; Jing, L.; Tian, C. *J. Hazard. Mater.* **2009**, *161*, 1122−1130.
(17) Toyoda, M.; Nanbu, Y.; Nakazawa, Y.; Hirano, M.; Inagaki, M. *Appl. Catal., B* **2004**, *49*, 227−232.
(18) Qi, G.; Yang, R. T. *Appl. Catal., B* **2003**, *44*, 217−225.
(19) Park, E.; Chin, S.; Kim, J.; Bae, G. N.; Jurng, J. *Powder Technol.* **2011**, *208*, 740−743.
(20) Chin, S.; Park, E.; Kim, M.; Jurng, J. *Powder Technol.* **2010**, *201*, 171−176.
(21) Chin, S.; Jurng, J.; Lee, J. H.; Moon, S. J. *Chemosphere* **2009**, *75*, 1206−1209.
(22) Yu, J.; Guo, F.; Wang, Y.; Zhu, J.; Liu, Y.; Su, F.; Gao, S.; Xu, G. *Appl. Catal., B* **2010**, *95*, 160−168.
(23) Wu, Z.; Jiang, B.; Liu, Y.; Zhao, W.; Guan, B. *J. Hazard. Mater.* **2007**, *145*, 488−494.
(24) Yang, T. T.; Bi, H. T.; Cheng, X. *Appl. Catal., B* **2011**, *102*, 163−71.
(25) Park, E.; Chin, S.; Jeong, J.; Jurng, J. *Microporous Mesoporous Mater.* **2012**, *163*, 96−101.
(26) Pena, D. A.; Uphade, B. S.; Smirniotis, P. G. *J. Catal.* **2004**, *221*, 421−431.
(27) Forzatti, P. *Catal. Today* **2000**, *62*, 51−65.
(28) Kim, Y. J.; Kwon, H. J.; Nam, I. S.; Choung, J. W.; Kil, J. K.; Kim, H. J.; Cha, M. S.; Yeo, G. K. *Catal. Today* **2010**, *151*, 244−250.
(29) Pecchi, G.; Reyes, P.; López, T.; Gómez, R.; Moreno, A.; Fierro, J. L. G. *J. Chem. Technol. Biotechnol.* **2002**, *77*, 944−949.
(30) Li, J.; Chang, H.; Ma, L.; Hao, J.; Yang, R. T. *Catal. Today* **2011**, *175*, 147−156.
(31) Crocoll, M.; Kureti, S.; Weisweiler, W. *J. Catal.* **2005**, *229*, 480−489.
(32) Huang, Y.; Gao, D.; Tong, Z.; Zhang, J.; Luo, H. *J. Nat. Gas Chem.* **2009**, *18*, 421−428.
(33) Delimaris, D.; Ioannides, T. *Appl. Catal., B* **2008**, *84*, 303−312.
(34) Wu, Z.; Jin, R.; Wang, H.; Liu, Y. *Catal. Commun.* **2009**, *10*, 935−939.
(35) Park, E.; Chin, S.; Kim, Y. S.; Bae, G. N.; Jurng, J. *Powder Technol.* **2012**, *233*, 131−136.
(36) Romano, E. J.; Schulz, K. H. *Appl. Surf. Sci.* **2005**, *246*, 262−270.
(37) Zhu, J.; Gao, F.; Dong, L.; Yu, W.; Qi, L.; Wang, Z.; Dong, L.; Chen, Y. *Appl. Catal., B* **2010**, *95*, 144−152.
(38) Bezrodna, T.; Puchkovska, G.; Shymanovska, V.; Baran, J.; Ratajczak, H. *J. Mol. Struct.* **2004**, *700*, 175−181.
(39) Labádi, I.; Horváth, L.; Kenessey, G.; Liptay, G. *J. Therm. Anal. Calorim.* **2006**, *83*, 247−251.
(40) Zhang, Y.; Zhao, X.; Xu, H.; Shen, K.; Zhou, C.; Jin, B.; Sun, K. *J. Colloid Interface Sci.* **2011**, *361*, 212−218.
(41) Kijlstra, W. S.; Brands, D. S.; Smit, H. I.; Poels, E. K.; Bliek, A. *J. Catal.* **1997**, *171*, 208−218.